Biochemical Pharmacology 201 (2022) 115069

Contents lists available at ScienceDirect

Biochemical Pharmacology

journal homepage: www.elsevier.com/locate/biochempharm

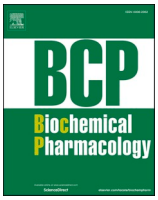

Thromboxane A_2 receptor activation via $G_{\alpha 13}$-RhoA/C-ROCK-LIMK2-dependent signal transduction inhibits angiogenic sprouting of human endothelial cells

Robert Eckenstaler [a,1], Anne Ripperger [a,1], Michael Hauke [a], Heike Braun [a], Süleyman Ergün [b], Edzard Schwedhelm [c], Ralf A. Benndorf [a,*]

[a] Martin-Luther-University Halle-Wittenberg, Department of Clinical Pharmacy and Pharmacotherapy, Halle (Saale), Germany
[b] Institute of Anatomy and Cell Biology, Julius-Maximilians-University, Würzburg, Germany
[c] Institute of Clinical Pharmacology and Toxicology, University Medical Center Hamburg-Eppendorf, Hamburg, Germany

ARTICLE INFO

Keywords:
Endothelial cells
Endothelial dysfunction
Angiogenic sprouting, cell tension,
Thromboxane A_2 receptor
$G_{\alpha 13}$
RhoA, RhoC, ROCK
LIMK2

ABSTRACT

We could previously show that thromboxane A_2 receptor (TP) activation inhibits the angiogenic capacity of human endothelial cells, but the underlying mechanisms remained unclear. Therefore, the aim of this study was to elucidate TP signal transduction pathways relevant to angiogenic sprouting of human endothelial cells. To clarify this matter, we used RNAi-mediated gene silencing as well as pharmacological inhibition of potential TP downstream targets in human umbilical vein endothelial cells (HUVEC) and VEGF-induced angiogenic sprouting of HUVEC spheroids *in vitro* as a functional read-out. In this experimental set-up, the TP agonist U-46619 completely blocked VEGF-induced angiogenic sprouting of HUVEC spheroids. Moreover, in live-cell analyses TP activation induced endothelial cell contraction, sprout retraction as well as endothelial cell tension and focal adhesion dysregulation of HUVEC. These effects were reversed by pharmacological TP inhibition or TP knockdown. Moreover, we identified a TP-$G_{\alpha 13}$-RhoA/C-ROCK-LIMK2-dependent signal transduction pathway to be relevant for U-46619-induced inhibition of VEGF-mediated HUVEC sprouting. In line with these results, U-46619-mediated TP activation potently induced RhoA and RhoC activity in live HUVEC as measured by FRET biosensors. Interestingly, pharmacological inhibition of ROCK and LIMK2 also normalized U-46619-induced endothelial cell tension and focal adhesion dysregulation of HUVEC. In summary, our work reveals mechanisms by which the TP may disturb angiogenic endothelial function in disease states associated with sustained endothelial TP activation.

1. Introduction

Angiogenesis, the formation of new blood vessels from pre-existing ones, is a tightly regulated process that plays a key role in pre- and postnatal development and is essential for physiological tissue function as well as tissue recovery from ischemic conditions in the postnatal organism [1,2]. Moreover, a dysfunctional vascular endothelium and an impaired response to angiogenic stimuli are commonly observed phenomena in cardiovascular high-risk patients and contribute to the pathogenesis and complications of cardiovascular disease [2,3]. During the process of angiogenesis, the usually quiescent vascular endothelium becomes locally activated by pro-angiogenic signals to allow for i.e. angiogenic sprouting, proliferation, migration, and vascular tube formation of endothelial cells in the surrounding tissue, thereby yielding *de novo* vascular structures that mature upon initiation of blood flow and recruitment of mural cells [1,2]. The process of angiogenesis is supported by a plethora of growth factors and signalling molecules. Among these, the vascular endothelial growth factor-A (VEGF-A/VEGF), has been identified as a key regulator of endothelial differentiation, vascular morphogenesis as well as physiological and pathophysiological angiogenesis [4,5]. In addition to its role in neovascularization, VEGF supports vascular endothelial cell survival and homeostasis [6] and

* Corresponding author at: Department of Clinical Pharmacy and Pharmacotherapy, Institute of Pharmacy, Martin-Luther-University Halle-Wittenberg, Wolfgang-Langenbeck-Str. 4, D-06120 Halle (Saale), Germany.
E-mail address: ralf.benndorf@pharmazie.uni-halle.de (R.A. Benndorf).
[1] Both authors contributed equally.

https://doi.org/10.1016/j.bcp.2022.115069
Received 8 March 2022; Received in revised form 26 April 2022; Accepted 27 April 2022
Available online 4 May 2022

contributes to the regulation of vascular tone and systemic blood pressure [7]. Thus, factors that counteract VEGF-related signal transduction in the vascular endothelium may not only impair the angiogenic response towards VEGF, but may also promote endothelial dysfunction and related complications.

Thromboxane A_2 (TxA_2) is an important mediator of platelet activation and regulator of vascular smooth muscle tone and contraction. It induces its effects via binding and activation of the heptahelical TxA_2 prostanoid receptor (TP/TBXA2R) [8]. In humans, two distinct isoforms of the TP, referred to as TP_α and TP_β, have been described which arise from alternative splicing and differ in the length of their C-terminus. In contrast, TP orthologues structurally similar to the human TP_α isoform are found in rodents [8]. Both human TP isoforms have been shown to couple to $G_{\alpha12/13}$, $G_{\alpha q/11}$, $G_{\alpha i/o}$ and possibly also $G_{\alpha s}$ [8]. Through these G_α subunits the TP may activate downstream effectors that are involved in cell adhesion, cytoskeletal remodelling, and cell tension, i.e. the small GTPases RhoA or RhoC as well as Rho and LIM kinases [8]. In addition to its role in hemostasis, the TP plays an important role in the vascular endothelium, where it promotes the development of endothelial dysfunction and cardiovascular disease and exerts pro-inflammatory, pro-apoptotic and anti-angiogenic effects [9–18], although also stimulatory effects of the TP on blood vessel formation and the angiogenic capacity of human endothelial cells have been described [19–21]. We and others have shown that the TP exerts angiostatic effects *in vitro*, *ex vivo*, and *in vivo* and limits the endothelial differentiation of angiogenic stem cell subsets [9–13,15–18]. Moreover, we recently uncovered a TP-driven and COX-2-dependent auto/paracrine positive feedback loop by which the receptor is able to trigger persistent self-activation independent of exogenous sources of TP ligands, thereby inducing endothelial dysfunction and impairing angiogenesis [22]. However, the downstream mechanisms by which TP activation leads to an impaired angiogenic response of human endothelial cells remained elusive. In the present study, we report that TP activation inhibits angiogenic sprouting of human endothelial cells primarily by activating a $G_{\alpha13}$-dependent signal transduction pathway involving RhoA and RhoC, Rho kinases (ROCK1 and ROCK2), LIM kinase 2 (LIMK2), and myosin II activation. In this context, live-cell analyses using FRET biosensors confirmed that U-46619-mediated TP activation potently induces RhoA and RhoC activity in HUVEC. In agreement with these observations, TP activation also induced endothelial cell contraction, sprout retraction as well as endothelial cell tension and disturbed focal adhesion dynamics of human endothelial cells, effects antagonized by pharmacological inhibition of ROCK, LIMK2, and myosin II activity. Other interesting findings of our work are that both knockdown of $G_{\alpha12}$ and in particular $G_{\alpha13}$ strongly promote spontaneous and VEGF-induced angiogenic sprouting of human endothelial cells, whereas pharmacological inhibition or knockdown of $G_{\alpha i/o}$ and $G_{\alpha q/11}$ abolishes VEGF-induced sprouting *in vitro*.

2. Materials and methods

2.1. Reagents

All chemicals and reagents were purchased from Sigma-Aldrich (St. Louis, USA), unless stated otherwise. Recombinant human VEGF-A was obtained from PeproTech Inc. (Rocky Hill, USA). U–46619, SQ 29,548 and blebbistatin were purchased from Cayman Chemical Europe (Tallin, Estland). The LIMK2 inhibitor LX-7101 was from Lexicon Pharmaceuticals (The Woodlands, USA), the LIMK1 inhibitor BMS4 was from Axon Medchem (Reston, USA), the ROCK1/2 inhibitor Y-27632 was from Santa Cruz Biotechnology (Dallas, USA).

Lentiviral plasmids LeGO-C2 and pHIV-SFiG-R1335 were kindly provided by Dr. Boris Fehse (Department of Stem Cell Transplantation, University Medical Center Hamburg-Eppendorf, Germany). For overexpression of the thromboxane A_2 receptor (TP) isoforms TP_α (NP_001051.1) and TP_β (NP_963998.2), the respective codon-optimized coding sequence (CDS) of both transcripts were cloned BamHI and NotI into the pHIV-SFiG-R1335 backbone. To allow for overexpression of dominant negative (T19N-mutated) RhoA (NP_001655.1) and RhoC (NP_001036143.1), 3x-HA-tagged and T19N-mutated, codon-optimized transcripts (RhoA, RhoC) were cloned into the pHIV-SFiG-R1335 backbone. ON-TARGET PLUS siRNAs directed against the TP (L-005740–00-0005), $G_{\alpha11}$ (L-010860–00-0005), ROCK1 (L-003536–00-0005), ROCK2 (L-004610–00-0005), LIMK1 (L-007730–00-0005) and LIMK2 (L-003311–00-0005) were purchased from Horizon Discovery (Waterbeach, UK). Non-targeting siRNA negative control (SIC001) and siRNA directed against $G_{\alpha q}$ (8012795211–0000110/120) were from Sigma-Aldrich (St. Louis, USA). For shRNA-mediated knockdown of $G_{\alpha12}$ (V2LHS_229790, V3LHS_388308), $G_{\alpha13}$ (V2LHS_204728, V3LHS_309624) commercially available shRNA sequences as well as a non-silencing shRNA control (RHS4346) pre-cloned into the GIPZ™ backbone were purchased from Horizon Discovery (Waterbeach, UK). psPAX2 (#12260), pMD2.G (#12259) and pmVenus(L68V)-mTurquoise2 (#60493) plasmids were obtained from addgene (Watertown, USA). The previously generated and validated [23] tension biosensor VinTS (addgene #26019) and its tailless control variant VinTL (addgene #26020), a variant that is incapable of coupling to cytoskeletal adapters of vinculin in vascular endothelial cells, were also obtained from addgene. RhoA and RhoC biosensors were a kind gift of Jaap van Buul (Sanquin Research, Amsterdam) and Yi Wu (Uconn Health, Farmington) [24].

2.2. Cell culture, transient transfection and lentiviral transduction of human endothelial cells

Human umbilical vein endothelial cells (HUVEC) were purchased from PromoCell (Heidelberg, Germany) and passaged in endothelial cell growth medium (PromoCell Heidelberg, Germany) on gelatin-coated multi-well plates or cell culture flasks according to the manufacturer's specifications at 37 °C in humidified air with 5% CO_2. HUVEC in passages 2–5 were used for the experiments. For transient transfection, HUVEC were detached and transiently transfected with non-targeting siRNA negative control or specific siRNAs (all at 100 nmol/L), respectively, using HUVEC-specific transfection kits and the nucleofector™ 2b device (all from Lonza, Basel, Switzerland) according to the instructions of the manufacturer. Afterwards, transfected cells were seeded in gelatin-coated 6-well plates at a density of 500,000 cells per well for 24 to 48 h prior to functional- and/or gene expression analyses. Transduction of HUVEC was performed with VSV-G-pseudotyped lentiviral particles derived from the pHIV-SFiG-1335 or GIPZ™ backbones. For stable lentiviral delivery of specific shRNAs and non-targeting shRNA control, HUVEC were infected with a multiplicity of infection (MOI) of 100. Infected cells were cultured for 24 to 72 h prior to functional or gene expression analyses depending on the experimental set up and as specified below. In all experiments, gene regulation levels were determined by real-time PCR or Western Blot analyses. Lentiviral transduction efficiencies were additionally determined by detecting GFP as a co-expressed reporter protein in endothelial cells. Efficiencies usually exceeded 90%.

2.3. Production, purification and titer determination of lentiviral vectors

Production, purification, and titration of lentiviral vectors was performed as described by Kutner *et al.* [25]. Shortly, HEK293T cells were seeded in 150 cm^2 dishes (Sarstedt, Nümbrecht, Germany) at a density of $8*10^6$ cells per dish in DMEM high-glucose medium supplemented with 10% FCS, 1% penicillin–streptomycin mix and 1% GlutaMAX (all Thermo Fisher Scientific, Waltham, USA). After 24 h, cells were used for transfection at a density of approximately 40%. 6 ml transfection mix per dish contains the transfer vector (60 μg), the VSV-G envelope-expressing plasmid pMD2.G (21 μg), the second-generation lentiviral packaging plasmid psPAX2 (39 μg), 2 M $CaCl_2$ (Roth, Karlsruhe,

Germany), water and 2x HEPES-buffered saline (Thermo Fisher Scientific, Waltham, USA) at a pH 7.07. Chloroquine at a final concentration of 25 μmol/mL was added to the medium right before transfection. Medium was changed once 20 h post-transfection. Two days after transfection, the cell supernatant was collected, centrifuged (500xg, 10 min) and filtered (pore size 0.45 μm, Sarstedt, Nümbrecht, Germany). The filtered supernatant was mixed in centrifuge beakers with 50% polyethylene glycol 6,000, 4 M NaCl (Roth, Karlsruhe, Germany) and 1x phosphate-buffered saline (Thermo Fisher Scientific, Waltham, USA). The mixture was stored at 4 °C for 90 min and the beakers were shaken every 30 min. To concentrate the lentiviral particles, suspension was centrifuged (7,000xg, 10 min 4 °C) and the pellet was resuspended in 50 mM Tris-HCl (Roth, Karlsruhe, Germany), pH 7.4. Lentiviral preparations were stored at −80 °C for further use.

Lentiviral vector titers were determined by flow cytometry (Attune® Acoustic Focusing flow cytometer, ThermoFisher Scientific, Waltham, USA). For this, $3*10^4$ HUVECs per well were plated in gelatin-coated 12-well plates (Greiner Greiner Bio-One, Frickenhausen, Germany) and transduced with certain amounts of virus suspension. 48 h post-transduction with known amount of virus suspension, cells were harvested and washed with 1x PBS/10% FCS. The number of eGFP-positive cells was measured by flow cytometry as described previously [26]. The virus titer was calculated according to the equation: Transducing Units (TU) $ml^{-1} = (F*D*N)/V$, where F is the percentage of GFP-positive cells, D is the fold dilution of virus used for transduction, N is the number of cells at the time of transduction and V is the volume of diluted virus added per well at transduction.

2.4. Angiogenic sprouting (endothelial cell spheroid) assay

Analyses of angiogenic sprouting from endothelial spheroids were carried out as described previously [27,28]. Briefly, HUVEC were resuspended in endothelial growth medium containing 20% methocel and were seeded dropwise into non-adherent culture dishes (squared culture plate, Greiner Bio-One, Frickenhausen, Germany) and allowed to form endothelial aggregates (spheroids) overnight in "hanging drops" containing 600 cells each at 37 °C in humidified air with 5% CO_2. In knockdown experiments, siRNA-treated HUVEC were seeded for 24 h after the transfection procedure prior to spheroid formation. For live-cell imaging of angiogenic sprouting, spheroids consisting of equal amounts of GFP- and mCherry-expressing cells were generated. Subsequently, 500 spheroids were embedded in 1000 μL of rat collagen containing 20% methocel and 10% FCS in non-adhesive 24-well plates (Greiner Bio-One, Frickenhausen, Germany) and kept in basal endothelial growth medium with or without VEGF (20 ng/mL) in presence or absence of the TP agonist U–46619 ($3x10^{-5}$ mol/L) as well as further pharmacological blockers for at least 24 h. As U–46619 had to be dissolved in ethanol-containing media, in these experiments both the basal and the VEGF-containing stimulation media were supplemented with equal amounts of ethanol (0.1%, Th. Geyer, Renningen, Germany). Angiogenic sprouting was quantified by measuring the cumulative sprout length of each spheroid using the NIS elements digital imaging software (Nikon, Tokyo, Japan), analyzing 10 spheroids per experimental group and experiment.

2.5. Live-cell imaging of angiogenic sprouting

Live cell imaging was performed using a Nikon A1R confocal microscope (Nikon, Tokyo, Japan) carrying lasers at 405, 457–514, 561, and 642 nm equipped with an O_2/CO_2 okolab cage incubator (okolab, Ottaviano, Italy). Time-lapse images of angiogenic sprouting from endothelial "mosaic" spheroids equally composed of EGFP- and mCherry-expressing HUVEC, respectively, were captured at 20 min intervals for up to 36 h using a CFI Plan Apochromat 10x objective (Nikon, Tokyo, Japan). To visualize the effect of TP stimulation on angiogenic sprouting of HUVEC, spheroids were kept with VEGF (20 ng/mL) in presence or absence of the TP agonist U–46619 ($3x10^{-5}$ mol/L).

2.6. Live-cell detection of endothelial cell tension (VinTS) as well as RhoA and RhoC activity using FRET-based biosensors

HUVECs were plated in a 96-well glass bottom plate (Greiner Bio-One, Frickenhausen, Germany) coated with 50 μg/ml fibronectin (Santa Cruz Technology, Dallas, USA) at a density of 10,000 cells per well and transfected with fluorescent FRET biosensors (VinTS, VinTL, RhoA, RhoC) using the TurboFect reagent (Thermo Fisher Scientific, Waltham, USA) according to the manufacturer's recommendations. FRET imaging was performed at 37 °C using a Nikon A1R confocal microscope equipped with a 60x oil immersion objective (plan apo lambda, Nikon, n.a. = 1.4), an argon laser (Melles Griot, Carlsbad, USA), a PMT/GaAsP detector unit (Nikon, Tokyo, Japan) and an O_2/CO_2 cage incubator (okolab, Ottaviano, Italy) as previously described [29]. Images were acquired and processed using the NIS-Elements FRET module (Nikon, Tokyo, Japan). FRET donors (RhoA/C: mCerulean3, VinTS/TL: mTFP1) were exited using the 457 nm laser line (argon laser) and fluorescence emission was detected in the spectral range of the donor (465–500 nm, DD image) and the acceptor (525–555 nm, DA image), respectively. In addition, FRET acceptors (RhoA/C and VinTS/TL: mVenus) were exited using the 514 nm laser line (argon laser) and detected in the spectral range of the acceptor (525–555 nm, AA image). Laser power and detector gain were set in a way to obtain best signal intensities while avoiding oversaturation of the images. Image settings were kept constant for each series of measurement and each image measured during subsequent time-lapse recordings. Calculation of FRET index was calibrated using donor and acceptor only samples (mCerulean3, mTFP1, mVenus) to determine the correction factors for donor crosstalk (α) and the acceptor's direct excitation (β) in the DA image. Images displaying the colour-coded FRET index were calculated as intensity of the corrected FRET image normalized by the intensity of the donor image according to the following formula (FRET index = (DA – αDD –βAA) / DD) * 100%).

2.7. Image processing

NIS Elements (Nikon, Tokyo, Japan) and Photoshop CS2 (Adobe, San José, USA) were used for image processing according to the Nature Research guidelines for image integrity and standards. In order to improve the visibility of fluorescence structures, brightness and contrast were uniformly increased over the entire image and the settings made were then applied identically to the image material of all experimental groups in one experiment. In the case of time-lapse imaging to compare morphological changes of fluorescent structures whose fluorescence intensities depend on the degree of transgene expression of the cell, image display was adapted so that comparable structures were similarly visible. The settings were then retained for each subsequent image during time-lapse imaging. In kymograph presentations, a representative 10x200 pixel portion of each time-lapse image was cut out and lined up one after the other to visualize changes over time in this region. For multi-colour merged images, the contrast and brightness of the individual colour channels were adjusted to optimize their visibility.

2.8. Real time RT-PCR

Total RNA was isolated, reverse transcribed, and analysed as described previously [30–33]. mRNA expression was quantified using the ABI 7500 Real-Time PCR System (Thermo Fisher Scientific, Waltham, USA). TaqMan reactions were carried out in 96-well plates according to the manufacturer's instructions using pre-made TaqMan™ Gene Expression Assays (probes) for the TP (Hs00169054_m1), $G_{\alpha 12}$ (Hs02863396_m1), $G_{\alpha q}$ (Hs00387073_m1), $G_{\alpha 11}$ (Hs01588833_m1), ROCK1 (Hs01127699_m1), ROCK2 (Hs00153074_m1), LIMK1 (Hs00242728_m1), LIMK2 (Hs00948689_m1), all from Thermo Fisher

Scientific (Waltham, USA). Hypoxanthine-guanine phosphoribosyl transferase 1 (HPRT1) was used as an endogenous control (Hs02800695_m1). All TaqMan™ Gene Expression Assays (probes) used in this study had been previously validated by the manufacturer, Thermo Fisher Scientific, and all probes span exons. We performed relative quantification of gene expression using the delta-delta Ct method [30].

2.9. Western Blot analysis

Western blot analysis of cellular protein levels was performed as previously described [31,34]. In brief, endothelial cells were lysed using pre-made lysis buffer (Cell Signaling Technology, Danvers, USA) containing 20 mmol/L Tris/HCl, pH 7.5, 1 mmol/L Na_2EDTA, 1 mmol/L EGTA, 150 mmol/L NaCl, 1% Triton X-100, 2,5mmol/L $Na_4P_2O_7$, 1 mmol/L b-glycerophosphate, 1 mM Na_3VO_4, and 1 µg/mL leupeptin and a premade protease and phosphatase inhibitors single use cocktail (Thermo Fisher Scientific, Waltham, USA). The lysates were subsequently centrifuged for 5 min, 4 °C, at 1,500xg to remove cell detritus. Equal amounts of proteins (30 µg/lane) were separated by SDS-PAGE and transferred to a nitrocellulose membrane. Afterwards, membranes were incubated with appropriate primary antibody solution and anti-β-Actin (clone AC-15) for normalization (Sigma Aldrich, St. Louis, USA; 1:5,000). The anti-HA antibody (C29F4; 1:1,000) was obtained from Cell Signaling Technology (Danvers, USA) and used for Western Blot analyses at the indicated dilutions or according to the manufacturer's instructions. The anti-$G_{\alpha 13}$ antibody (6F6-B5; 1:500) was from Santa Cruz Biotechnology (Dallas, USA). Antibodies directed against the TP_α and TP_β isoform were purchased from Cayman Chemical (Ann Arbor, USA; TP_α; #10004452; 1:500) and Genscript Biotech (Piscataway Township, USA; custom-made NP963998; 1:500). Bound antibodies were detected by peroxidase-conjugated secondary antibodies and the ECL system (Amersham Bioscience, Amersham, UK).

2.10. Statistical analyses

Statistical analyses were performed using one-way analysis of variance followed by Sidak's multiple comparisons test or the unpaired student's *t*-test. For statistical analyses the Graph Pad Prism 6 software package was used (Graph Pad Software, Inc., La Jolla, USA). Data were expressed as mean ± standard deviation (SD), standard error of the mean (S.E.M.), or as indicated otherwise. Probability values were considered significant at a $p < 0.05$.

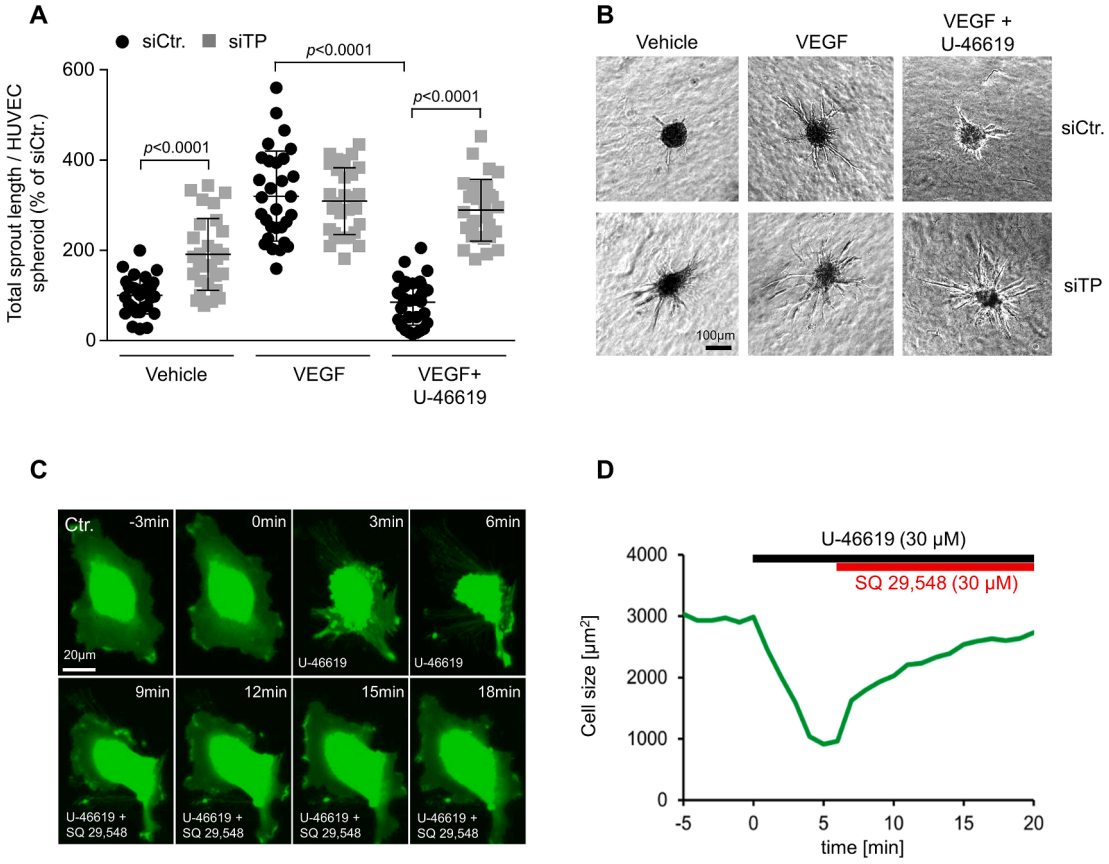

Fig. 1. Pharmacological TP activation inhibits VEGF-induced HUVEC sprouting and induces endothelial cell contraction. Human umbilical vein endothelial cells (HUVEC) were transfected with non-targeting control siRNA (siCtr.) or siRNA directed against both variants (TPα and TPβ) of the human thromboxane A_2 receptor (siTP). After spheroid-formation and spheroid-embedding, sprouting of the cells was analyzed in presence of vehicle control (Vehicle), 20 ng/mL VEGF (VEGF), or 20 ng/mL VEGF plus 30 µmol/L U-46619 (VEGF + U-46619), respectively. U-46619 represents a stable TP agonist and prostaglandin H_2 analogue. A-B) TP activation using U–46619 ($3x10^{-5}$ mol/L) antagonizes VEGF-induced sprouting from HUVEC spheroids *in vitro*, whereas siRNA-mediated knockdown of the TP reverses the inhibitory effect of U-46619 on VEGF-induced HUVEC sprouting and significantly increases basal sprouting of HUVEC spheroids. All data are shown as scatter plots with mean ± SD (n = 29–30). Absolute angiogenic sprouting values (mean values ± standard deviation of the total sprout length in µm) were: 442 ± 421 (siCtr. - Vehicle), 1514 ± 907 (siCtr. - VEGF), 462 ± 308 (siCtr. - VEGF + U-46619), 746 ± 272 (siTP - Vehicle), 1343 ± 800 (siTP - VEGF), 1265 ± 694 (siTP - VEGF + U-46619). B) Representative microscopic pictures of HUVEC spheroid sprouts. C-D) Live cell imaging demonstrates that U-46619-induced TP activation causes contraction of HUVEC in two-dimensional culture *in vitro*. Moreover, cell contraction is partly reversed by concomitant TP antagonism using SQ 29,548 ($3x10^{-5}$ mol/L).

3. Results

3.1. Pharmacological TP activation inhibits VEGF-induced angiogenic sprouting from HUVEC spheroids and induces contraction of HUVEC in two-dimensional culture

We had previously shown that the stable PGH_2 analogue and TP agonist U-46619 reduces VEGF-induced migration and tube formation of human coronary artery and dermal microvascular endothelial cells (HCAEC, HDMEC) *in vitro* [13], but its effect on VEGF-induced angiogenic sprouting of human endothelial cells remained unknown. Therefore, we first studied the effect of U-46619 on VEGF-induced angiogenic sprouting of human umbilical vein endothelial cells (HUVEC) spheroids. In this experimental setting, U-46619 ($3x10^{-5}$ mol/L) completely blocked VEGF-induced HUVEC sprouting (Fig. 1A,B). In live-cell imaging analyses using mosaic HUVEC spheroids consisting of HUVEC either expressing the green fluorescent reporter GFP or the red fluorescent reporter mCherry we could substantiate the morphological basis of this finding and observed that U-46619 induced a more frequent retraction of early sprouts and thus, inhibited sprout formation and elongation (Supplemental Video 1). In line with these observations, U-46619 also induced endothelial cell contraction in cultured HUVEC, an effect that was reversed by concomitant TP antagonism using SQ 29,548 (Fig. 1C, D).

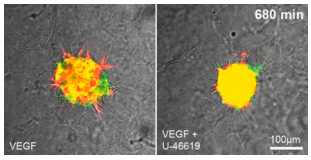

Video 1. Control spheroids, consisting of GFP- and mCherry-expressing control HUVEC, show the dynamic formation of a balanced and regular sprout morphology during stimulation with VEGF (20 ng/mL), thereby revealing typical characteristics of angiogenic sprout formation, i.e. tip and stalk cell competition. However, concomitant stimulation with the TP agonist U-46619 causes a more frequent retraction of early sprouts and thus, inhibits sprout formation and elongation.

3.2. Identification of downstream effectors of TP-induced anti-angiogenic effects in HUVEC

To identify anti-angiogenic signal transduction pathways activated by the TP, we used systematic gene silencing and pharmacological inhibition of potential TP downstream targets in HUVEC as well as VEGF-induced angiogenic sprouting from HUVEC spheroids in presence or absence of U-46619 ($3x10^{-5}$ mol/L) as a functional read-out. As shown in Fig. 1A-B, the TP agonist completely inhibited VEGF-induced sprouting of HUVEC spheroids. Importantly, the anti-angiogenic effect of U-46619 on HUVEC sprouting was completely blocked by siRNA-mediated TP knockdown (Fig. 1A,B; for representative RNAi knockdown efficacies of the TP or TP-related targets please see Fig. 2A-G), emphasizing the central role of the TP for the biological activity of this stable PGH_2 analogue. Next, we analysed the role of G proteins $G_{\alpha12}$, $G_{\alpha13}$, $G_{\alpha q/11}$ and $G_{\alpha i/o}$ which have been previously described to couple to the TP [8] in the anti-angiogenic effect induced by U-46619. For this purpose, we used RNAi-mediated gene silencing ($G_{\alpha12}$, $G_{\alpha13}$, $G_{\alpha q/11}$) or the $G_{\alpha i/o}$ inhibitor pertussis toxin (PTX, 10 ng/mL) to selectively disrupt G protein signal transduction. The inhibitory effect of U-46619 on angiogenic HUVEC sprouting was virtually inverted by shRNA-mediated knockdown of $G_{\alpha13}$ but not by knockdown of $G_{\alpha12}$ (Fig. 3A-B). These results could be replicated by using second independent shRNAs directed against $G_{\alpha12}$ and $G_{\alpha13}$, respectively (Fig. 3C). In contrast, the effect of U-46619 was not significantly affected by siRNA-mediated knockdown of $G_{\alpha q/11}$ or pharmacological $G_{\alpha i/o}$ inhibition (Fig. 3D,E). Moreover, both $G_{\alpha q/11}$ knockdown and $G_{\alpha i/o}$ protein inhibition significantly reduced VEGF-induced angiogenic sprouting (Fig. 3D,E), whereas both $G_{\alpha12}$ and $G_{\alpha13}$ knockdown enhanced basal and VEGF-induced angiogenic sprouting of HUVEC spheroids (Fig. 3A-C). Next, we analysed the role of $G_{\alpha12/13}$ downstream effectors, namely the small GTPases RhoA and RhoC as well as the Rho effectors Rho kinase 1 and 2 (ROCK1, ROCK2) in TP-related signal transduction in HUVEC. In this context, co-overexpression of dominant-negative variants of $G_{\alpha13}$ downstream effectors RhoA and RhoC completely reversed the inhibitory effect of U–46619 on VEGF-induced HUVEC sprouting (Fig. 4A-D). Moreover, co-overexpression of

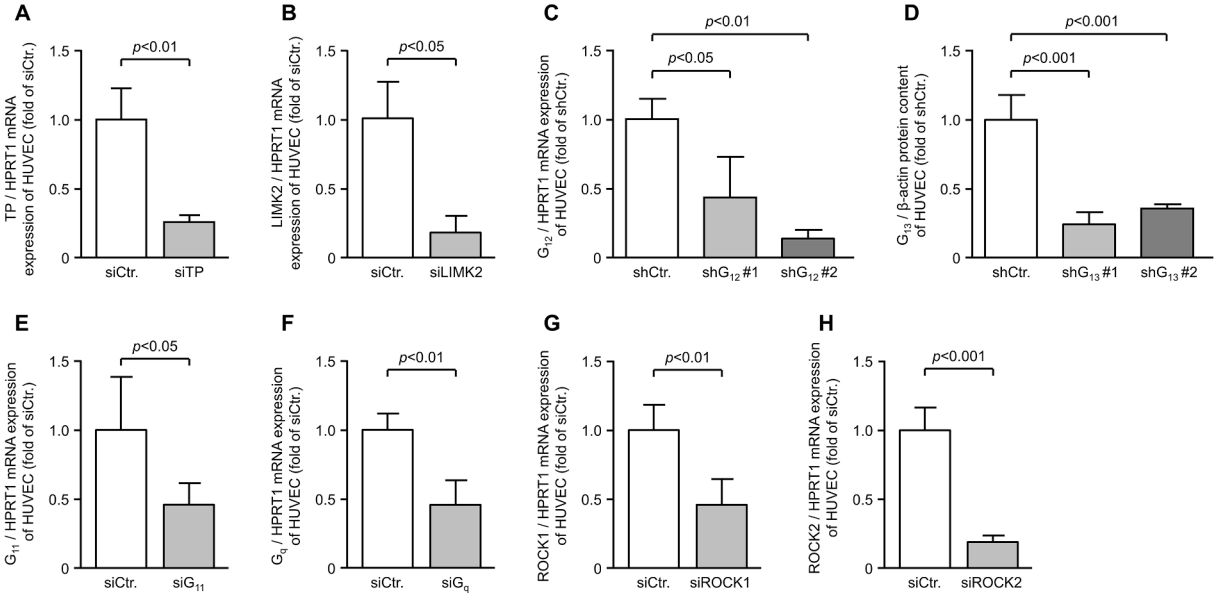

Fig. 2. Representative efficacy of siRNA- or shRNA-mediated knockdown of the TP or various TP-related targets in human umbilical vein endothelial cells (HUVEC). Knockdown of the TP and its potential downstream targets in HUVEC was performed either by transient transfection of the cells with specific siRNAs directed against the TP (siTP, A), LIMK2 (siLIMK2, B), G_{11} (siG_{11}, E), G_q (siG_q, F), ROCK1 (siROCK1, G), or ROCK2 (siROCK2, H), or non-targeting siRNA control (siCtr.) or by lentiviral delivery of specific shRNAs directed against G_{12} (shG_{12} #1, shG_{12} #2, C) or G_{13} (shG_{13} #1, shG_{13} #2, D) and by delivery of non-targeting shRNA control (shCtr.). Knockdown of the TP (n = 3; A), LIMK2 (LIMK2; n = 3; B), G_{12} (n = 3; C), G_{13} (n = 3–6; D), G_{11} (n = 4; E), G_q (n = 4; F), ROCK1 (n = 4; G), and ROCK2 (n = 4; H) resulted in a significant decrease of either the respective mRNA, quantified by real-time RT-PCR (A-C, E-H), or resulted in a significant decrease of the G_{13} protein content, quantified by Western Blot analysis (D), as indicated. Data are shown as mean ± standard deviation.

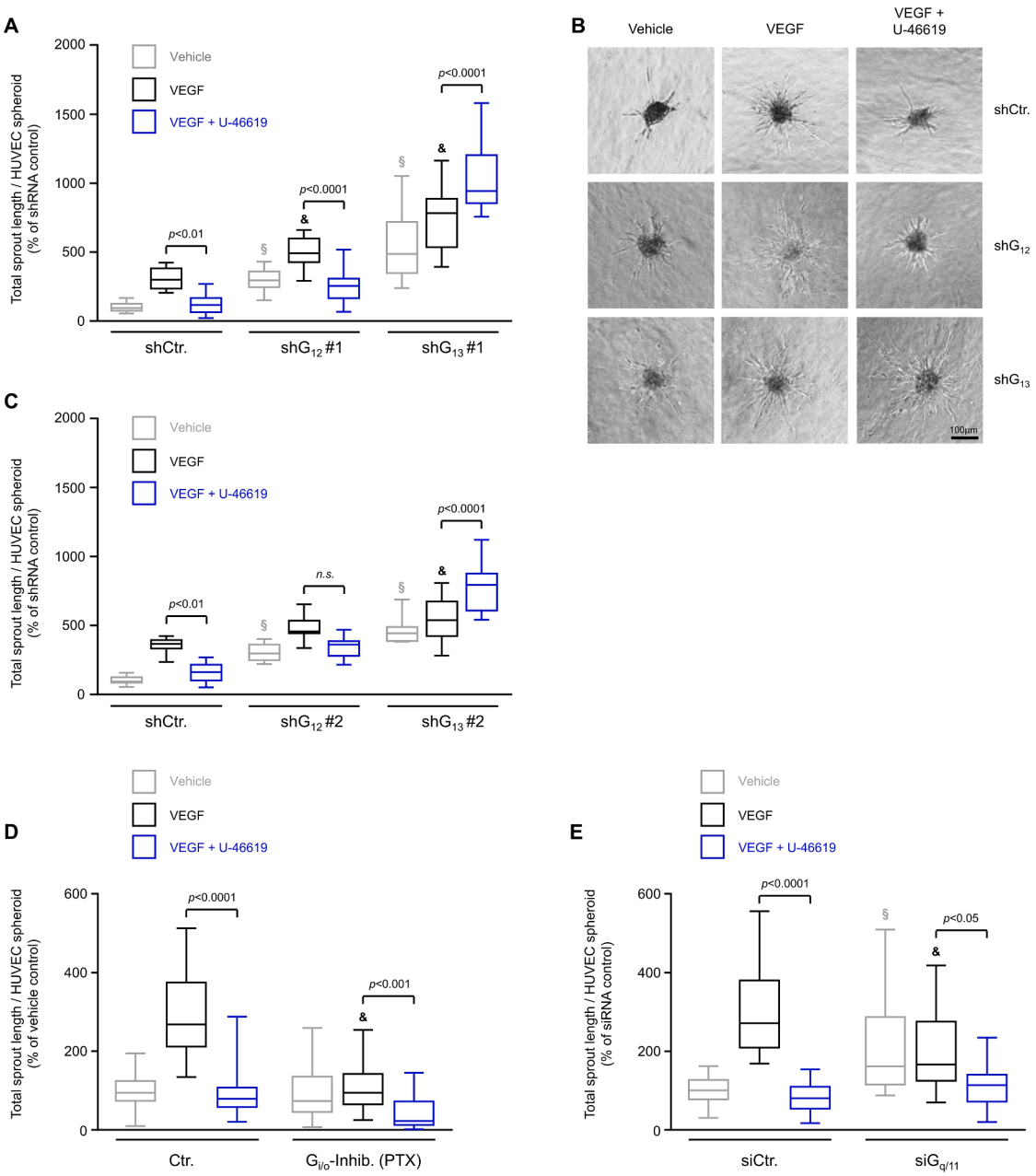

Fig. 3. TP-mediated inhibition of angiogenic HUVEC sprouting is mediated via G_{13}-dependent, but not G_{12}-, $G_{q/11}$-, or $G_{i/o}$-related signal transduction. Human umbilical vein endothelial cells (HUVEC) were lentivirally transduced with vectors expressing non-targeting control shRNA (shCtr.) or shRNA directed against G_{12} (two independent constructs: shG_{12} #1, shG_{12} #2, A-C) or G_{13} (two independent constructs: shG_{13} #1, shG_{13} #2, A-C). After spheroid-formation and spheroid-embedding, sprouting of the cells was analyzed in presence of vehicle control (Vehicle), 20 ng/mL VEGF (VEGF), or 20 ng/mL VEGF plus 30 µmol/L U-46619 (VEGF + U-46619), respectively. U-46619 represents a stable TP agonist and prostaglandin H_2 analogue. A-C) shRNA-mediated knockdown of either $G_{\alpha12}$ or $G_{\alpha13}$ induces basal and VEGF-induced angiogenic sprouting of HUVEC spheroids. Moreover, knockdown of $G_{\alpha13}$ but not of $G_{\alpha12}$ virtually inverses the inhibitory effect of the TP agonist U–46619 on VEGF-induced HUVEC angiogenic sprouting. (A). All data derived from sprouting assays are expressed as median with 25% and 75% percentiles (n = 20). Absolute values (mean values ± standard deviation of the total sprout length in µm) were: 540 ± 196 (shCtr. - Vehicle Ctr.), 1701 ± 634 (shCtr. - VEGF), 707 ± 474 (shCtr. - VEGF + U-46619), 1590 ± 510 (shG_{12} #1 - Vehicle Ctr.), 2786 ± 988 (shG_{12} #1 - VEGF), 1321 ± 526 (shG_{12} #1 - VEGF + U-46619), 2710 ± 901 (shG_{13} #1 - Vehicle Ctr.), 3910 ± 1004 (shG_{13} #1 - VEGF), 5450 ± 974 (shG_{13} #1 - VEGF + U-46619). § $p < 0.001$ vs. basal sprouting of vehicle-treated shRNA control (shCtr.) HUVEC. & $p < 0.001$ vs. VEGF-treated shRNA control (shCtr.) HUVEC. B) Representative microscopic pictures of HUVEC spheroid sprouts. C) Findings shown in Fig. 3A were replicated using a second independent set of shRNAs (shG_{12} #2 and shG_{13} #2; n = 10). Absolute values (mean values ± standard deviation of the total sprout length in µm) were: 631 ± 192 (shCtr. - Vehicle Ctr.), 2252 ± 362 (shCtr. - VEGF), 1021 ± 470 (shCtr. - VEGF + U-46619), 2162 ± 422 (shG_{12} #2 - Vehicle Ctr.), 2516 ± 834 (shG_{12} #2 - VEGF), 1571 ± 367 (shG_{12} #2 - VEGF + U-46619), 2059 ± 410 (shG_{13} #2 - Vehicle Ctr.), 2424 ± 789 (shG_{13} #2 - VEGF), 3565 ± 881 (shG_{13} #2 - VEGF + U-46619). § $p < 0.01$ vs. basal sprouting of vehicle-treated shRNA control (shCtr.) HUVEC. & $p < 0.01$ vs. VEGF-treated shRNA control (shCtr.) HUVEC. In contrast, inhibition of $G_{i/o}$ proteins using pertussis toxin (PTX; 10 ng/mL; D; n = 40) or knockdown of $G_{q/11}$ using siRNA (E; n = 20) do not affect the inhibitory effect of U-46619 on HUVEC angiogenic sprouting, but reduce VEGF-induced sprouting *per se*. Absolute values (mean values ± standard deviation of the total sprout length in µm) were: 789 ± 356 (Ctr. - vehicle Ctr.), 2201 ± 604 (Ctr. - VEGF), 673 ± 287 (Ctr. - VEGF + U-46619), 773 ± 661 (PTX – vehicle Ctr.), 938 ± 734 (PTX – VEGF), 498 ± 435 (PTX – VEGF + U-46619). 430 ± 216 (siCtr. - vehicle Ctr.), 1152 ± 273 (siCtr. - VEGF), 354 ± 182 (siCtr. - VEGF + U-46619), 789 ± 275 ($siG_{q/11}$. - vehicle Ctr.), 713 ± 205 ($siG_{q/11}$ - VEGF), 447 ± 189 ($siG_{q/11}$ - VEGF + U-46619). § $p < 0.001$ vs. basal sprouting of respective negative control HUVEC. & $p < 0.001$ vs. VEGF-induced sprouting of respective negative control HUVEC.

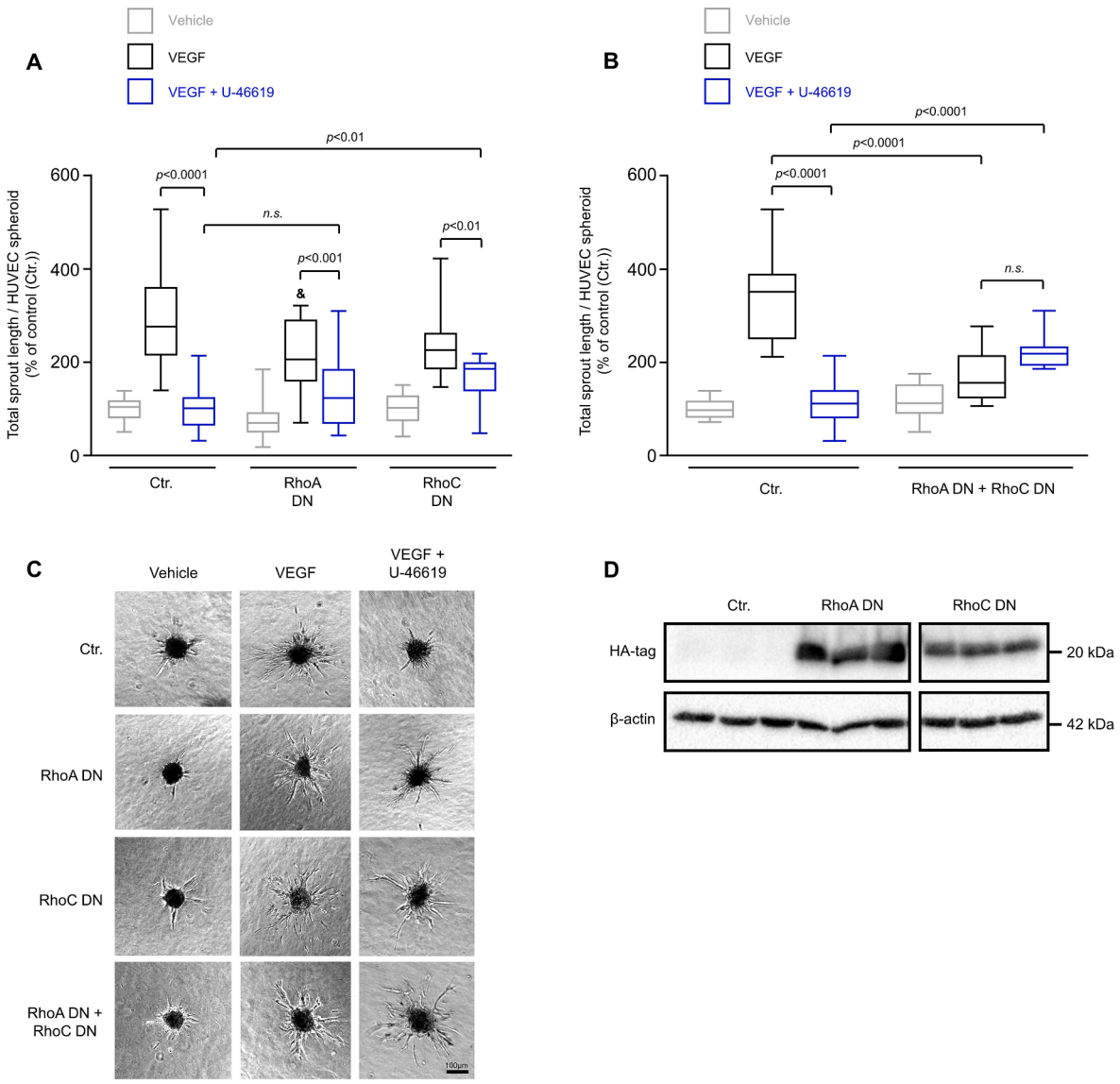

Fig. 4. TP activation inhibits angiogenic sprouting from HUVEC spheroids via RhoA and RhoC-dependent signal transduction. Human umbilical vein endothelial cells (HUVEC) were lentivirally transduced with a control vector (Ctr., A-D) or vectors expressing dominant-negative RhoA (RhoA DN, A,C,D), dominant-negative RhoC (RhoC DN, A,C,D) or both dominant-negative RhoA and dominant-negative RhoC (RhoA DN + RhoC DN, B-C). After spheroid-formation and spheroid-embedding, sprouting of the cells was analyzed in presence of vehicle control (Vehicle), 20 ng/mL VEGF (VEGF), or 20 ng/mL VEGF plus 30 µmol/L U-46619 (VEGF + U-46619), respectively. U-46619 represents a stable TP agonist and prostaglandin H_2 analogue. A) Expression of either dominant-negative RhoA (RhoA DN) or dominant-negative RhoC variants (RhoC DN) in HUVEC does not fully reverse U-46619-induced inhibition of HUVEC sprouting *in vitro* (n = 20). Absolute values (mean values ± standard deviation of the total sprout length in µm) were: 1460 ± 593 (Ctr. - vehicle), 4026 ± 1140 (Ctr. VEGF), 1416 ± 590 (Ctr. VEGF + U-46619), 1036 ± 437 (RhoA DN – vehicle), 2926 ± 902, (RhoA DN – VEGF), 1849 ± 924 (RhoA DN– VEGF + U-46619), 1416 ± 549 RhoC DN – vehicle), 3359 ± 952, (RhoC DN – VEGF), 2529 ± 1173 (RhoC DN – VEGF + U-46619). & $p < 0.001$ vs. VEGF-induced sprouting of negative control HUVEC. All data are expressed as median with 25% and 75% percentiles. B) Expression of both dominant-negative RhoA and dominant-negative RhoC variants (RhoA DN + RhoC DN) in HUVEC fully reverses U-46619-induced inhibition of HUVEC sprouting *in vitro* (n = 10). Absolute values (mean values ± standard deviation of the total sprout length in µm) were: 1033 ± 214 (Ctr. - vehicle), 3532 ± 979 (Ctr. VEGF), 1180 ± 558 (Ctr. VEGF + U-46619), 1223 ± 410 (RhoA DN + RhoC DN – vehicle), 1761 ± 599, (RhoA DN + RhoC DN – VEGF), 2300 ± 368 (RhoA DN + RhoC DN – VEGF + U-46619). C) Representative microscopic pictures of HUVEC spheroid sprouts. D) Western Blot analysis of HA-tagged RhoA DN and RhoC DN expression in HUVEC after lentiviral transduction.

dominant-negative RhoA and RhoC significantly reduced VEGF-induced angiogenic sprouting, thereby indicating a role of both GTPases in this process (Fig. 4B). To study the effect of TP activation on RhoA and RhoC activity in HUVEC, we used validated RhoA and RhoC FRET biosensors (Fig. 5A-C). In line with the previous observations, U–46619 TP-dependently induced a steady RhoA and RhoC activation in live HUVEC (Fig. 5D,E and Supplemental Video 2). This activation could be blocked by pharmacological inhibition of the TP using SQ 29,548 (Fig. 5G,I) and was more pronounced in HUVEC lentivirally transduced to overexpress either the TP_α or the TP_β isoform (Fig. 5F,H; see Fig. 5J for verification of TP overexpression), indicating that both isoforms participate in RhoA and RhoC activation in endothelial cells. In contrast, U–46619 did not affect the FRET efficiency of a cytosolic FRET positive control tandem (Fig. 5K), suggesting that U-46619-mediated contraction of HUVEC should not affect the FRET efficiency of the biosensors. Moreover, U–46619-induced inhibition of angiogenic sprouting in HUVEC were significantly reduced by siRNA-mediated knockdown (Fig. 6A-E) or by pharmacological inhibition of Rho downstream effectors ROCK1 and ROCK2, LIMK2 (but not LIMK1; Fig. 6F) and myosin II (Fig. 6G). Taken together, these data suggest that the TP negatively

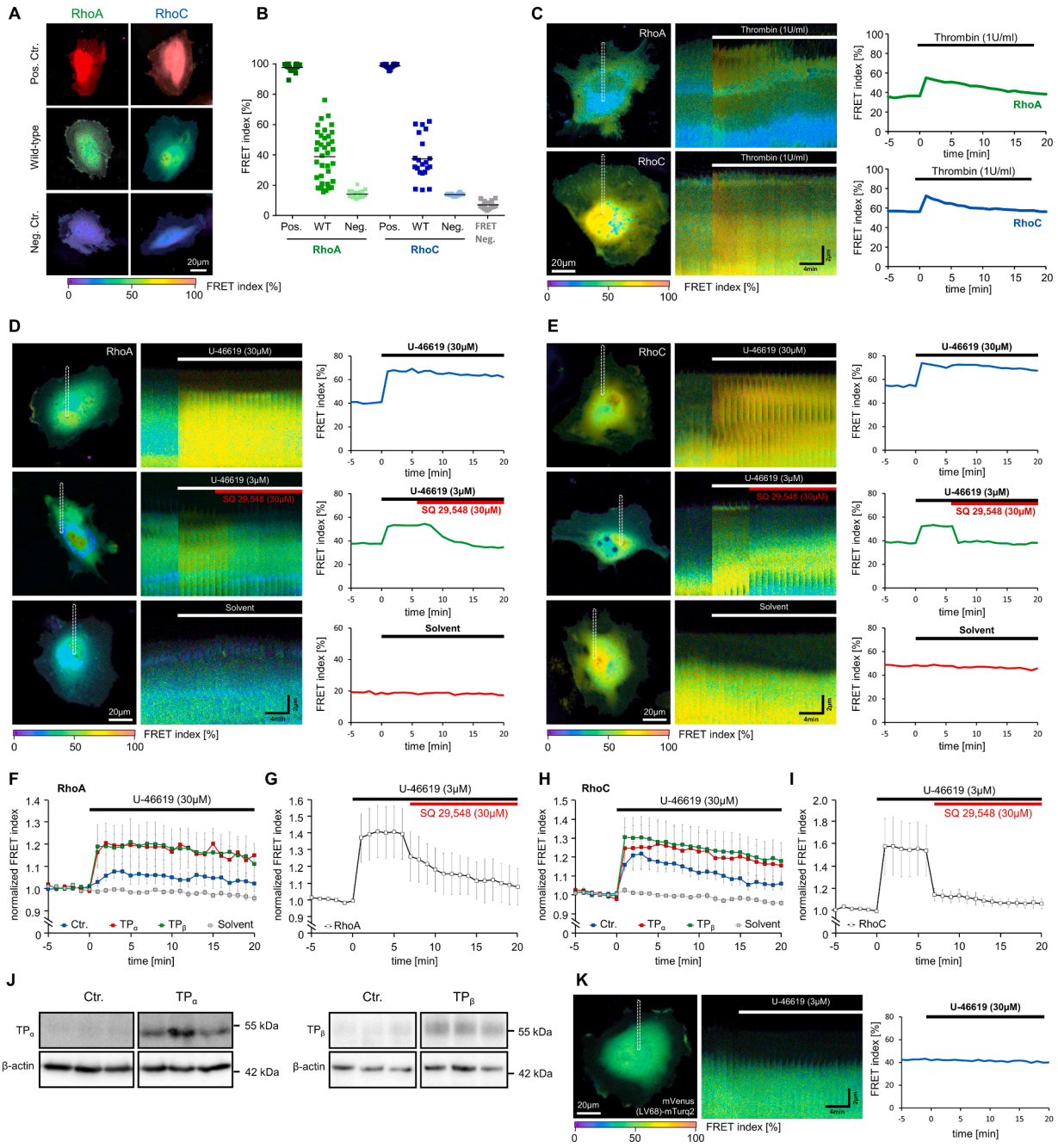

Fig. 5. TP activation increases RhoA and RhoC activity in human endothelial cells. A-B) Validation of the dynamic range of RhoA and RhoC FRET biosensors transiently expressed in HUVEC. The FRET index was measured in cells transfected with wild-type (WT, FRET values correlate with the activity status of RhoA/RhoC), constitutively active (Pos. Ctr., FRET values of the maximum active RhoA/C) or dominant-negative (Neg. Ctr., FRET values of inactive RhoA/C) Rho biosensor variants in HUVEC (n = 10–19). FRET negative control (FRET neg.) represents non-specific FRET between the separated donor (mCerulean3) and acceptor (mVenus) transfected in HUVECs. C) Validation of the responsiveness of RhoA/C biosensors to external stimuli (1U/ml Thrombin). Representative kymographs of a section of the cell and resulting single cell traces of the whole cell showing spatio-temporal thrombin-induced transient RhoA and RhoC activation in single HUVEC expressing either the WT RhoA or the WT RhoC biosensor, respectively. D,E) The TP agonist U–46619 ($3x10^{-6}$ to $3x10^{-5}$ mol/L) induces a long-lasting RhoA and RhoC activation in HUVEC that can be reverted by subsequent application of TP antagonist 29,548 ($3x10^{-5}$ mol/L). The application of the solvent of U-46619 did not alter FRET. Left panel (D,E): Representative endothelial cells expressing the RhoA (D) or RhoC (E) FRET biosensor. Middle panel (D,E): Representative kymographs showing TP-related activation of RhoA (D) or RhoC (E) in U-46619-stimulated HUVEC. Right panel (D,E): Corresponding trace of the FRET index of the whole cell indicating TP-dependent Rho activation. F,H) RhoA and RhoC activation is more pronounced in HUVEC lentivirally transduced to overexpress either the TP_α or the TP_β isoform as compared with control-transduced HUVEC. Data are shown as mean ± S.E.M. (RhoA starting values of non-normalized FRET index in %: Ctr: 49.4 ± 7.0, n = 6; TP_α: 43.3 ± 7.0, n = 6; TP_β: 57.2 ± 4.4, n = 6; solvent: 48.0 ± 6.3, n = 7 / RhoC starting values of non-normalized FRET index in %: Ctr: 42.4 ± 3.6, n = 9; TP_α: 34.3 ± 5.1, n = 8; TP_β: 38.6 ± 5.4, n = 9; solvent: 48.6 ± 6.8, n = 9). G, I) U–46619-induced RhoA and RhoC activation is antagonized by the TP antagonist SQ 29,548 ($3x10^{-5}$ mol/L). Data are shown as mean ± S.E.M. (starting values of non-normalized FRET index in %: RhoA: 44.3 ± 4.8; RhoC: 30.5 ± 4.9, both n = 5). J) Overexpression of either the TP_α or the TP_β isoform in HUVEC using stable lentiviral gene transfer was validated using Western Blot analyses. K) TP activation with U-46619 ($3x10^{-5}$ mol/L) does not affect FRET index of a FRET positive control tandem (pmVenus(L68V)-mTurquoise2) transiently expressed in HUVEC.

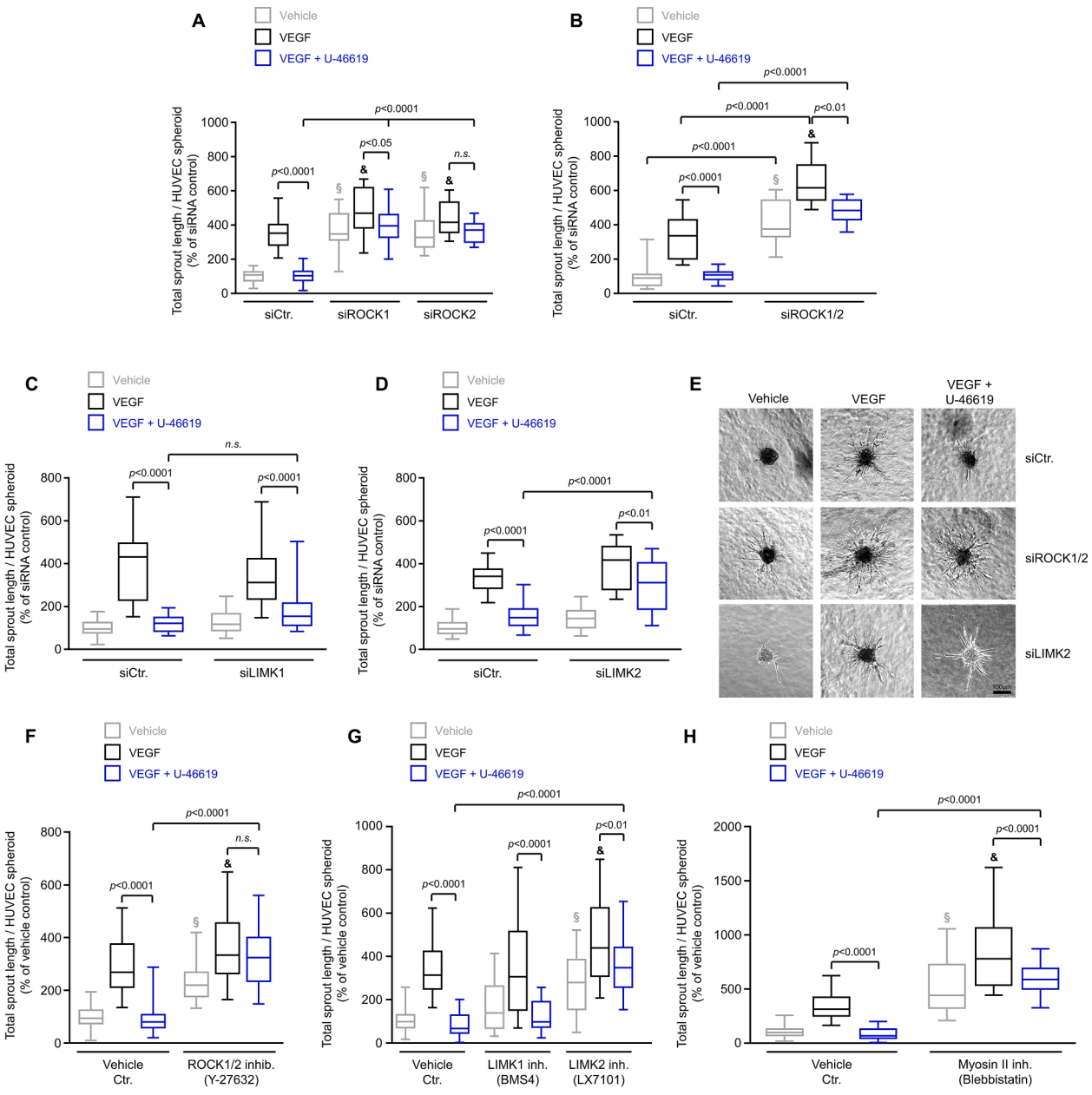

(caption on next page)

Fig. 6. Rho kinases, LIM kinase 2, and myosin II activity play a role in TP-mediated inhibition of VEGF-induced HUVEC spheroid sprouting. Human umbilical vein endothelial cells (HUVEC) were transfected with non-targeting control siRNA (siCtr.) or siRNA directed against the human ROCK1 (siROCK1, A), ROCK2 (siROCK2, A), ROCK1 and ROCK2 (siROCK1/2, B, E), LIMK1 (siLIMK1, C), or LIMK2 (siLIMK2, D-E). After spheroid-formation and spheroid-embedding, sprouting of the cells was analyzed in presence of vehicle control (Vehicle), 20 ng/mL VEGF (VEGF), or 20 ng/mL VEGF plus 30 μmol/L U-46619 (VEGF + U-46619), respectively. U-46619 represents a stable TP agonist and prostaglandin H_2 analogue. A) siRNA-mediated knockdown of either Rho kinase 1 (ROCK1) or Rho kinase 2 (ROCK2) attenuates the inhibitory effect of U–46119 on VEGF-induced HUVEC spheroid sprouting and strongly increases both spontaneous and VEGF-induced HUVEC sprouting. All data are expressed as median with 25% and 75% percentiles (n = 20). Absolute values (mean values ± standard deviation of the total sprout length in μm) were: 286 ± 104 (siCtr.- vehicle), 1019 ± 249 (siCtr. - VEGF), 301 ± 135 (siCtr. - VEGF + U-46619), 1069 ± 294 (siROCK1 – vehicle), 1359 ± 369, (siROCK1 – VEGF), 1132 ± 257 (siROCK1– VEGF + U-46619), 995 ± 271 (siROCK2 – vehicle), 1261 ± 289 (siROCK2 – VEGF), 1037 ± 176 (siROCK2 – VEGF + U-46619). § $p < 0.0001$ vs. spontaneous sprouting of negative control HUVEC. & $p < 0.05$ vs. VEGF-induced sprouting of negative control HUVEC. B) Similar effects are observed when knockdown of both ROCK1 and ROCK2 is performed in HUVEC (n = 10). Absolute values (mean values ± standard deviation of the total sprout length in μm) were: 754 ± 622 (siCtr. - vehicle), 2503 ± 941 (siCtr. VEGF), 792 ± 301 (siCtr. VEGF + U-46619), 3163 ± 985 (siROCK1 + 2 – vehicle), 4861 ± 914, (siROCK1 + 2 – VEGF), 3632 ± 529 (siROCK1 + 2 – VEGF + U-46619). § $p < 0.0001$ vs. spontaneous sprouting of negative control HUVEC. & $p < 0.0001$ vs. VEGF-induced sprouting of negative control HUVEC. C) siRNA-mediated knockdown of LIMK1 does not significantly affect TP-induced reduction of VEGF-induced HUVEC sprouting (n = 30). Absolute values (mean values ± standard deviation of the total sprout length in μm) were: 620 ± 442 (siCtr. - vehicle), 1920 ± 476 (siCtr. - VEGF), 622 ± 220 (siCtr. - VEGF + U-46619), 692 ± 322 (siLIMK1 – vehicle), 1713 ± 617, (siLIMK1 – VEGF), 900 ± 373 (siLIMK1 – VEGF + U-46619). D) In contrast, knockdown of LIMK2 significantly attenuates the inhibitory effect of U–46619 on VEGF-induced HUVEC spheroid sprouting (n = 20). Absolute values (mean values ± standard deviation of the total sprout length in μm) were: 561 ± 191 (siCtr. - vehicle), 1861 ± 397 (siCtr. - VEGF), 842 ± 293 (siCtr. - VEGF + U-46619), 768 ± 275 (siLIMK2 – vehicle), 2164 ± 484, (siLIMK2 – VEGF), 1654 ± 561 (siLIMK2 – VEGF + U-46619). E) Representative microscopic pictures of HUVEC spheroid sprouts. F-G) Replication of knockdown results using specific pharmacological inhibitors of ROCK1/2 (Y-27632; 10 μmol/L), LIMK1 (BMS4; 0.5 μmol/L), and LIMK2 (LX7101; 3 μmol/L). F) Pharmacological inhibition of ROCK1/2 reverses the inhibitory effect of U-46619 on VEGF-induced angiogenic sprouting. The effect of Y-27632 was studied in the same experiments as that of the $G_{i/o}$ inhibitor pertussis toxin and tested against the same control group as shown in Fig. 3D. All data are expressed as median with 25% and 75% percentiles (n = 40). Absolute values (mean values ± standard deviation of the total sprout length in μm) were: 789 ± 356 (vehicle), 2201 ± 604 (VEGF), 673 ± 287 (VEGF + U-46619), 1789 ± 590 (Y-27632 - vehicle), 2711 ± 850 (Y-27632 – VEGF), 2432 ± 635 (Y-27632 – VEGF + U-46619). G) Inhibition of LIMK2, but not LIMK1 significantly reduces the inhibitory effect of U-46619 on VEGF-induced HUVEC spheroid sprouting. § $p < 0.0001$ vs. spontaneous sprouting of negative control HUVEC. & $p < 0.01$ vs. VEGF-induced sprouting of negative control HUVEC. All data are expressed as median with 25% and 75% percentiles (n = 30 (BMS4-treated cells); n = 40 (all other groups)). Absolute values (mean values ± standard deviation of the total sprout length in μm) were: 400 ± 232 (Ctr. - vehicle), 1323 ± 508 (Ctr. - VEGF), 352 ± 264 (Ctr. - VEGF + U-46619), 588 ± 378 (BMS4 - vehicle), 1092 ± 567 (BMS4 – VEGF), 412 ± 204 (BMS4 – VEGF + U-46619), 1019 ± 462 (LX7101 - vehicle), 1741 ± 540 (LX7101 – VEGF), 1414 ± 559 (LX7101 – VEGF + U-46619). § $p < 0.0001$ vs. spontaneous sprouting of vehicle control HUVEC. & $p < 0.0001$ vs. VEGF-induced sprouting of vehicle control HUVEC. H) Moreover, pharmacological inhibition of myosin II activity using blebbistatin (30 μmol/L) weakens TP-induced inhibition of VEGF-induced HUVEC sprouting and strongly increases spontaneous and VEGF-induced HUVEC sprouting in the absence of U-46619. All data are expressed as median with 25% and 75% percentiles (n = 40). Absolute values (mean values ± standard deviation of the total sprout length in μm) were: 400 ± 232 (Ctr. - vehicle), 1323 ± 508 (Ctr. - VEGF), 352 ± 264 (Ctr. - VEGF + U-46619), 2099 ± 875 (BMS4 - vehicle), 3183 ± 865 (BMS4 – VEGF), 2435 ± 537 (BMS4 – VEGF + U-46619).The effect of blebbistatin was studied in the same experiments as that of BMS4, and LX7101 and tested against the same control group as shown in G). However, the results are presented separately in H) because blebbistatin greatly increased spontaneous and VEGF-induced sprouting, so the scale had to be adjusted accordingly. § $p < 0.0001$ vs. spontaneous sprouting of vehicle control HUVEC. & $p < 0.0001$ vs. VEGF-induced sprouting of vehicle control HUVEC.

affects the angiogenic capacity of human endothelial cells via activation of a G_{13}-RhoA/RhoC-ROCK-LIMK2- and myosin II-dependent pathway that has been described to be involved in the regulation of the actin cytoskeleton, cell tension, and focal adhesion dynamics.

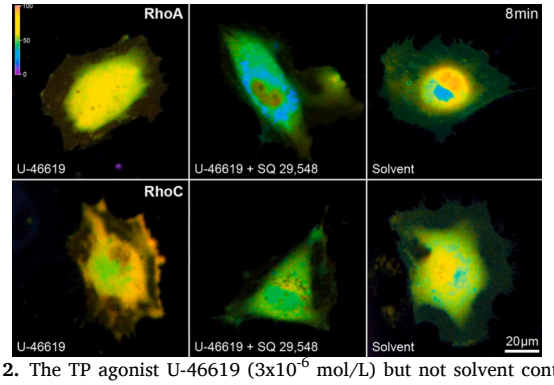

Video 2. The TP agonist U-46619 ($3x10^{-6}$ mol/L) but not solvent control induces a prolonged activation of both RhoA and RhoC in HUVEC indicated by an increase in FRET index of RhoA and RhoC FRET biosensors as shown exemplarily for TP_{β}-overexpressing HUVEC. Moreover, U-46619-induced RhoA and RhoC activation, respectively, is reversed by the TP antagonist SQ 29,548 ($3x10^{-5}$ mol/L).

3.3. TP activation increases cellular tension and affects focal adhesion dynamics of human endothelial cells

Our analyses of TP-related signal transduction as well as our microscopic live-cell analyses suggested that pharmacological TP activation generated cellular tension to induce contraction of cultured endothelial cells and endothelial spheroid sprout retraction. To substantiate these observations, we analysed endothelial cell tension generated at focal adhesions and focal adhesion dynamics of HUVEC using a live-cell setup and a vinculin-based FRET biosensor (VinTS) which indicates increasing cell tension by a reduction in FRET efficiency. In these experiments, we observed that the TP agonist U–46619 increased tension at focal adhesions in HUVEC (Fig. 7A,B and Supplemental Video 3). The U-46619-induced increase in cell tension again was blocked by either pharmacological TP inhibition (Fig. 7D) or pharmacological inhibition of actomyosin regulators ROCK and LIMK2 (Fig. 7E,F). In contrast, U–46619 did not affect the FRET efficiency of a tailless biosensor control variant (VinTL; Fig. 7G,H), indicating that functional coupling of the sensor to cytoskeletal adapters is necessary to indicate FRET-dependent changes in cell tension. TP stimulation also increased the average size of vinculin-containing focal adhesions in HUVEC, in both VinTS- and VinTL-expressing HUVEC (Fig. 7C, I and Supplemental Video 4) and thus independently of the coupling of the

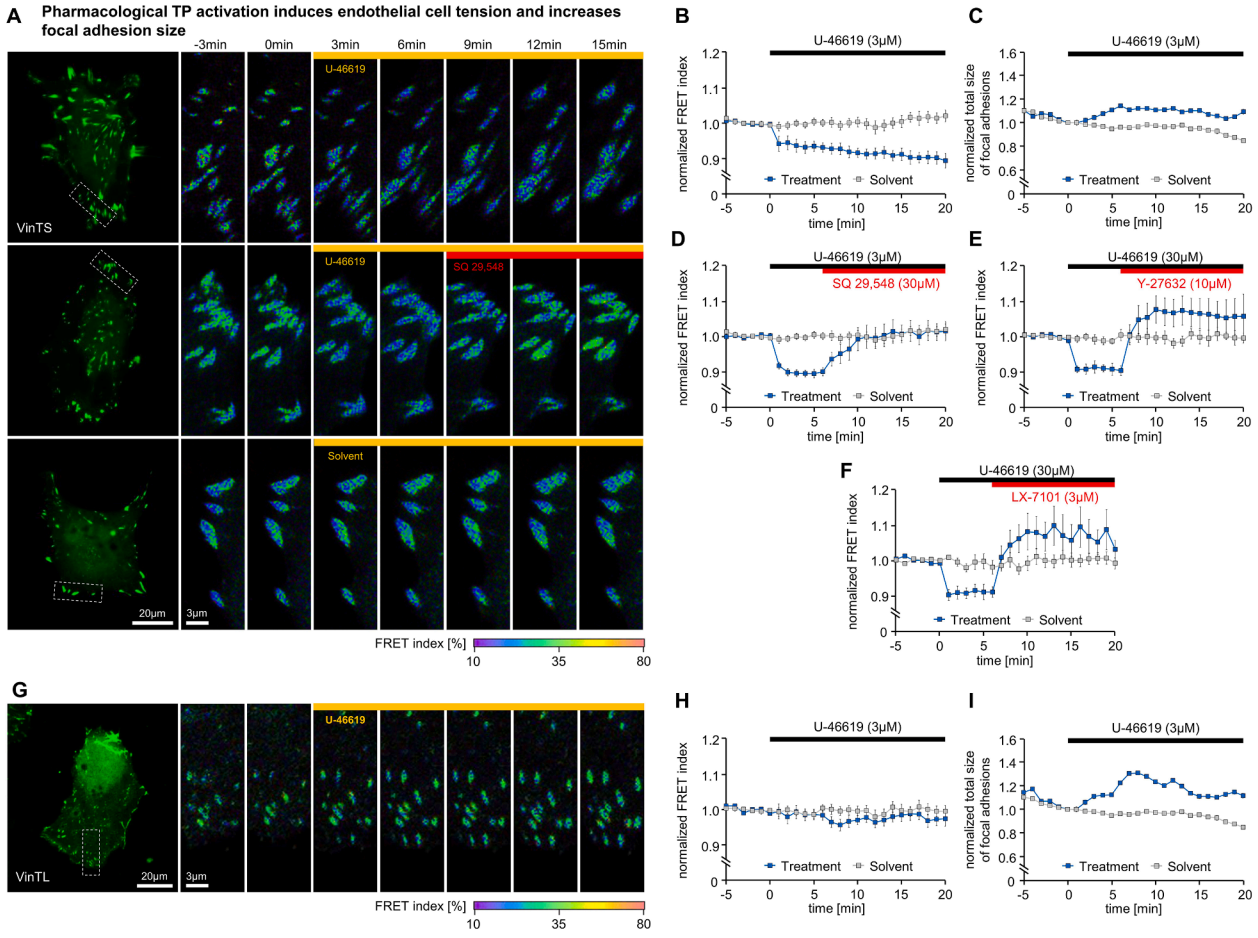

Fig. 7. Pharmacological activation of the TP induces cellular tension of human endothelial cells *in vitro*. A) Representative microscopic pictures of an endothelial cell transiently expressing the VinTS biosensor treated with solvent control or U–46619 ($3x10^{-6}$ mol/L) in presence or absence of SQ 29,548 ($3x10^{-5}$ mol/L), respectively. B) The TP agonist U–46619 ($3x10^{-6}$ mol/L) but not solvent control increases cellular tension at focal adhesions in HUVEC *in vitro* as evidenced by a decrease in FRET index of VinTS due to a more pronounced cell tension-induced separation of both involved fluorophores along their elastic linker (starting values of non-normalized FRET index in %: Treatment: 30.0 ± 1.1, n = 11; Solvent: 33.1 ± 4.7, n = 6). U–46619 also increases the total area size of vinculin-containing focal adhesions in these cells (C; starting values of non-normalized total size of focal adhesions in μm^2: Treatment: 81.1 ± 13.0, n = 11; Solvent: 91.7 ± 11.8, n = 7). D-F) Furthermore, the increase in cellular tension is reversed by pharmacological TP inhibition using SQ 29,548 (D; $3x10^{-5}$ mol/L, starting values of non-normalized FRET index in %: treatment: 27.4 ± 1.7, n = 8 vs. solvent: 33.1 ± 4.7, n = 6) or inhibitors for actomyosin regulators ROCK (E; 10 µM Y-27632, starting values of non-normalized FRET index in %: treatment: 27.8 ± 0.9, n = 7 vs. solvent: 27.4 ± 0.9, n = 8) and LIMK2 (F; 3 µM LX7101, starting values of non-normalized FRET index in %: treatment: 27.8 ± 0.8, n = 6 vs. solvent: 28.8 ± 0.8, n = 7). Data are shown as mean ± S.E.M.. G-H) The TP agonist U-46619 ($3x10^{-6}$ mol/L) does not affect the FRET index of a tailless variant (VinTL) of the cell tension biosensor (VinTS) expressed in HUVEC in. Dynamic changes in focal adhesion morphology and associated FRET index of a representative endothelial cell are shown (G). In contrast to VinTS, the VinTL variant is unable to couple to cytoskeletal adapter proteins of vinculin thereby being unaffected by changes in cell tension (starting values of non-normalized FRET index in %: Treatment: 33.7 ± 0.7, n = 3 vs. solvent: 27.4 ± 0.9, n = 8). Nonetheless, U-46619 supports the maturation/growth of vinculin-containing focal adhesions (starting values of non-normalized total size of focal adhesions in μm^2: Treatment: 108.7 ± 50.3, n = 4; Solvent: 91.7 ± 11.8, n = 7) in VinTL-expressing HUVEC as well (I).

sensor to the actin cytoskeleton. Taken together, these results therefore suggest that TP activation leads to an increase in cell tension and a change in the dynamics of focal adhesions in human endothelial cells.

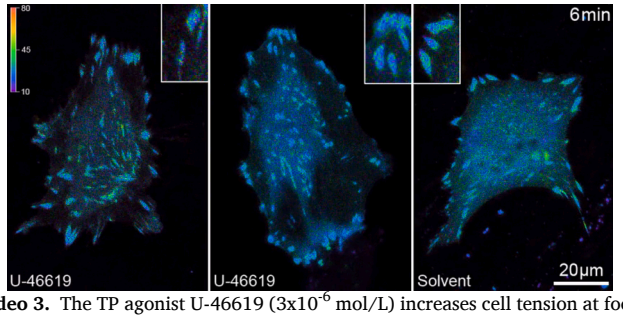

Video 3. The TP agonist U-46619 ($3x10^{-6}$ mol/L) increases cell tension at focal adhesions in HUVEC in two-dimensional culture and as evidenced by a decrease in FRET efficiency of a vinculin-based tension biosensor (VinTS). TP-related tension generation is effectively inhibited by addition of the TP antagonist SQ-29548 ($3x10^{-5}$ mol/L). In contrast, solvent control (0,01% ethanol) does not affect cellular tension during the measurement period.

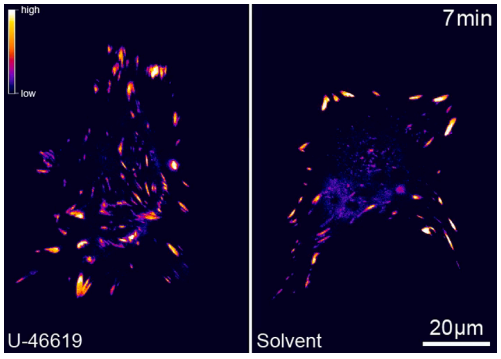

Video 4. The TP agonist U-46619 ($3x10^{-6}$ mol/L) supports the assembly and maturation of focal adhesions in HUVEC in two-dimensional culture. Focal adhesion dynamics were visualized in living HUVEC additionally transfected with the vinculin-based tension biosensor (VinTS). mVenus fluorescence intensity of VinTS is visualized in a false colour-coded fashion ranging from light yellow (high intensity) to blue (low intensity).

4. Discussion

The thromboxane A_2 (TxA_2) prostanoid receptor (TP) is an important mediator of vascular hemostasis that also acts as a relevant effector in the pathogenesis of endothelial dysfunction and cardiovascular disease [8]. In addition, we and further groups have demonstrated previously that TP activation impairs the angiogenic capacity of vascular endothelial cells *in vitro*, inhibits angiogenesis *in vivo*, and counteracts the potential of angiogenic stem cell subsets to promote neovascularization *in vitro* and *in vivo* [9–13,15–18]. Moreover, we have recently discovered a TP-driven cyclooxygenase-2-dependent feedback loop that directly links upregulation of either the TP_α or the TP_β isoform to angiostatic TP signal transduction in endothelial cells, most likely via cyclooxygenase-2-mediated increased prostaglandin H_2 biosynthesis and related constitutive, auto-/paracrine TP activation that also increases endothelial cell tension and induces focal adhesion dysregulation [22]. In the latter work, we also demonstrated in global transcriptome analyses that increased expression and associated sustained activation of the TP (both the TP_α and TP_β isoform) in human endothelial cells downregulates numerous important angiogenic mediators such as VEGFR-2 and eNOS, whereas it promotes the expression of angiogenesis inhibitors such as thrombospondin-1 and thus may favour the development of an anti-angiogenic phenotype of human endothelial cells [22]. It has to be mentioned in this regard that other groups report a supportive role of the TP in the process of angiogenesis [19–21,35]. For instance, global TP knockout in mice was associated with decreased neovascularization in the hindlimb ischemia model of angiogenesis [19]. Moreover, this phenotype could be rescued by transplantation of TP-expressing (wild-type) bone marrow in TP-deficient mice and was shown to depend on TP-induced P-selectin expression in platelets [19]. In contrast to these results, another group observed neither an effect of pharmacological TP inhibition (S18886, terutroban) nor of pharmacological cyclooxygenase (COX) inhibition (aspirin) on neovessel formation in the same experimental model [35]. Nonetheless, both TP and COX inhibition reduced angiotensin II-induced neovascularization in this regard, thereby indicating a role of thromboxane A_2 and the TP in transducing pro-angiogenic angiotensin II signals *in vivo* [35]. In this context, however, we could show that endothelial-specific deletion of the TP increased VEGF- and bFGF-induced blood vessel formation in the murine Matrigel plug assay *in vivo*, confirming our findings in human endothelial cells that the TP is a negative regulator of endothelial cell-mediated angiogenesis [22]. Thus, one possible explanation for the partially contradictory results on the influence of TP on angiogenesis could be that the TP exerts cell-type-specific effects on this process, with the receptor inducing anti-angiogenic signals in the murine vascular endothelium and human endothelial cells.

On the mechanistic level, however, only little information is available on how TP agonists, such as the stable PGH_2 analogue U-46619, inhibit angiogenic endothelial cell functions. For example, Asthon and colleagues demonstrated negative interactions with VEGF-induced signal transduction in human endothelial cells. Here, they showed that different TP agonists induced apoptosis and inhibited VEGF-dependent migration and tube formation of human endothelial cells by mechanisms involving inhibition of VEGF-induced protein kinase B/Akt-eNOS or focal adhesion kinase (FAK) activation [10,15]. Furthermore, the same group revealed that activation of the TP_β isoform blocked ligand-induced FGFR1 internalization and consequently FGF-2-induced migration of human endothelial cells *in vitro* by reducing FGFR1 internalization via a thrombospondin-1-dependent mechanism [9]. In addition, we demonstrated in previous work that TP-dependent inhibition of chemotactic endothelial cell migration *in vitro* was reversed by concomitant pharmacological ROCK1/2 inhibition [13]. In line with these observations, we also showed recently that increased endothelial TP expression *per se* induced RhoA activity (both TP isoforms) in HUVEC and that pharmacological inhibition of RhoA downstream effectors ROCK1/2, LIMK2, and myosin II was able to reduce the inhibitory effect of TP overexpression on the angiogenic function of human endothelial cells *in vitro* [22].

Despite the existing evidence that TP impairs angiogenic function of human endothelial cells, a systematic mechanistic workup of anti-angiogenic TP downstream effectors had not yet been performed. Therefore, this was the main objective of the present study. To uncover anti-angiogenic signal transduction pathways activated by the TP, we performed systematic gene silencing and pharmacological inhibition of potential TP downstream targets in HUVEC and subsequently analyzed the impact of the TP agonist U-46619 on VEGF-induced angiogenic sprouting of HUVEC spheroids as a functional read-out. This angiogenic model is well established in many laboratories and the employed human endothelial cells (HUVEC) are commonly studied in this context. First, we were able to demonstrate that U-46619 completely blocked VEGF-induced sprouting from native HUVEC spheroids and that neither treatment with negative control siRNA nor shRNA affected VEGF-induced angiogenic sprouting and the inhibitory effects of U-46619 in our experimental set-up. Moreover, we could show that U-46619 induces endothelial cell contraction of HUVEC in a TP-dependent manner. We also confirmed in HUVEC the significance of the TP for the inhibitory effect of U-46619 on HUVEC spheroid sprouting via specific knockdown of the receptor. As the heptahelical TP has been described to couple to G proteins such as $G_{\alpha12/13}$, $G_{\alpha q/11}$, and $G_{\alpha i/o}$ [8], we then evaluated the contribution of these signalling molecules to the effects of TP activation. We observed that neither knockdown of $G_{\alpha q/11}$ nor inhibition of $G_{\alpha i/o}$ proteins affected the inhibitory effect of U-46619 on endothelial

sprouting in our experimental system. Yet, these G proteins appeared to play an important role in VEGF-related angiogenic sprouting, since it was strongly reduced by $G_{\alpha i/o}$ inhibition and considerably impaired by $G_{\alpha q/11}$ knockdown, respectively. To our knowledge, we are the first to describe an inhibitory effect of $G_{\alpha i/o}$ inhibition on VEGF-induced endothelial sprouting, although the mechanistic background of this effect remains to be clarified. Nonetheless, involvement of $G_{\alpha i/o}$ proteins in VEGF-induced angiogenesis and (lymph)angiogenic actions of further mediators, i.e. sphingosine-1-phosphate, has been described [36,37], which may help to elucidate the mechanistic interplay between the VEGF-A-VEGFR-2 axis and $G_{\alpha i/o}$ proteins in the context of angiogenic sprouting. In contrast, the important role of $G_{\alpha q/11}$ in VEGF-induced angiogenesis has been described before [38] and hence, we were able to confirm the role of $G_{\alpha q/11}$ in the angiogenic response of endothelial cells to VEGF. Next, we evaluated the role of $G_{\alpha 12}$ and $G_{\alpha 13}$ proteins in anti-angiogenic TP signal transduction by using an shRNA-mediated knockdown approach. Interestingly, G_{13} virtually inverted the anti-angiogenic effect of U-46619, such that U-46619 no longer inhibited VEGF-induced angiogenic sprouting but highly significantly enhanced it. In contrast, $G_{\alpha 12}$ knockdown apparently did not antagonize the effect of the TP agonist. These data to the best of our knowledge are the first to uncover that $G_{\alpha 13}$ is responsible for transducing the inhibitory actions of the TP on endothelial sprouting. Our results also indicate for the first time that $G_{\alpha 13}$ may serve as a "molecular switch" that determines whether TP activation exerts anti- or pro-angiogenic effects in human endothelial cells. Our findings are in line with data from other groups which report that the TP activation primarily induces interaction of the receptor with $G_{\alpha 13}$ and not $G_{\alpha 12}$ [39,40]. Furthermore, we observed that both $G_{\alpha 13}$ and to a lesser extent also $G_{\alpha 12}$ knockdown strongly enhanced basal but also VEGF-induced sprouting from HUVEC spheroids. These findings are in contrast to previous findings that identify $G_{\alpha 13}$ as a critical regulator of VEGFR-2 expression and VEGF-induced angiogenesis *in vitro* (HUVEC) and in mice *in vivo* [41]. The reason for this discrepancy is unclear. Nonetheless, also further groups have reported an involvement of $G_{\alpha 12/13}$ in anti-angiogenic signal transduction in HUVEC as well as an enhanced basal sprouting from HUVEC spheroids after inhibition of $G_{\alpha 12/13}$ *in vitro* [42]. Downstream of $G_{\alpha 13}$ we identified RhoA and RhoC, ROCK1/2 as well as the ROCK effectors LIMK2 and myosin II to be relevant for the transduction of U-46619-induced effects on HUVEC sprouting. In line with these findings, U-46619 induced a steady activation of both RhoA and RhoC and this activation was even more pronounced when HUVEC were engineered to overexpress either the TP_{α} or TP_{β} isoform, respectively. In addition, knockdown or inhibition of ROCK and LIMK2 again induced basal and VEGF-induced sprouting from endothelial spheroids, thereby suggesting that basal activity of the $G_{\alpha 13}$-RhoA/C-ROCK-LIMK2 and myosin II-dependent pathway may serve to limit endothelial sprouting by increasing actomyosin-related cellular tension in the absence or presence of pro-angiogenic stimuli such as VEGF. Indeed, we demonstrated that TP activation in live endothelial cells induces an increase in cell tension at focal adhesions, which depends on the activation of ROCK and LIMK2.

In conclusion, our work reveals that U-46619-mediated TP activation increases cellular tension and inhibits angiogenic sprouting of human endothelial cells via $G_{\alpha 13}$-RhoA/C-ROCK1/2-LIMK2 and myosin II-dependent signal transduction, a pathway of which the basal activity additionally appears to limit angiogenic sprouting of endothelial cells *per se*.

5. Limitations of the study

Despite the good comparability of our study with other studies in terms of the angiogenic model and primary human endothelial cells (HUVEC) used for our functional studies, our study has clear limitations. Indeed, it is an *in vitro*-only study that was designed to explore VEGF-antagonistic anti-angiogenic TP-induced signal transduction pathways. Therefore, it is possible that the behavior of these cells *in vitro* is not representative of processes that occur in perfused blood vessels in the living organism. Thus, based on our results, further *ex vivo* and *in vivo* studies should be performed in the future to validate the obtained results in clinically relevant models of physiology and pathophysiology and to investigate their potential therapeutic relevance.

CRediT authorship contribution statement

Robert Eckenstaler: Methodology, Investigation, Formal analysis, Writing – original draft, Visualization. **Anne Ripperger:** Methodology, Investigation, Formal analysis. **Michael Hauke:** Methodology, Investigation, Formal analysis. **Heike Braun:** Methodology, Investigation, Formal analysis. **Süleyman Ergün:** Writing – review & editing. **Edzard Schwedhelm:** Writing – review & editing. **Ralf A. Benndorf:** Conceptualization, Formal analysis, Writing – original draft, Visualization, Supervision, Project administration, Funding acquisition. All authors read and approved the final manuscript.

Acknowledgements

The authors gratefully acknowledge the expert technical assistance of Dorothea Frenzel. This work was supported by the Deutsche Forschungsgemeinschaft (DFG INST 271/342-1 and BE 3246/6-1) and by the European Regional Development Fund of the European Commission (W21029490) to R.A.B.

References

[1] P. Carmeliet, R.K. Jain, Molecular mechanisms and clinical applications of angiogenesis, Nature 473 (7347) (2011) 298–307.
[2] M. Potente, H. Gerhardt, P. Carmeliet, Basic and therapeutic aspects of angiogenesis, Cell 146 (6) (2011) 873–887.
[3] P.N. Hopkins, Molecular biology of atherosclerosis, Physiol Rev 93 (3) (2013) 1317–1542.
[4] M. Shibuya, Vascular Endothelial Growth Factor (VEGF) and Its Receptor (VEGFR) Signaling in Angiogenesis: A Crucial Target for Anti- and Pro-Angiogenic Therapies, Genes Cancer 2 (12) (2011) 1097–1105.
[5] M. Simons, E. Gordon, L. Claesson-Welsh, Mechanisms and regulation of endothelial VEGF receptor signalling, Nat Rev Mol Cell Biol 17 (10) (2016) 611–625.
[6] S. Lee, T.T. Chen, C.L. Barber, M.C. Jordan, J. Murdock, S. Desai, N. Ferrara, A. Nagy, K.P. Roos, M.L. Iruela-Arispe, Autocrine VEGF signaling is required for vascular homeostasis, Cell 130 (4) (2007) 691–703.
[7] C.S. Facemire, A.B. Nixon, R. Griffiths, H. Hurwitz, T.M. Coffman, Vascular endothelial growth factor receptor 2 controls blood pressure by regulating nitric oxide synthase expression, Hypertension 54 (3) (2009) 652–658.
[8] J. Bauer, A. Ripperger, S. Frantz, S. Ergün, E. Schwedhelm, R.A. Benndorf, Pathophysiology of isoprostanes in the cardiovascular system: implications of isoprostane-mediated thromboxane A2 receptor activation, Br J Pharmacol 171 (13) (2014) 3115–3131.
[9] A.W. Ashton, Y. Cheng, A. Helisch, J.A. Ware, Thromboxane A2 receptor agonists antagonize the proangiogenic effects of fibroblast growth factor-2: role of receptor internalization, thrombospondin-1, and alpha(v)beta3, Circ Res 94 (6) (2004) 735–742.
[10] A.W. Ashton, J.A. Ware, Thromboxane A2 receptor signaling inhibits vascular endothelial growth factor-induced endothelial cell differentiation and migration, Circ Res 95 (4) (2004) 372–379.
[11] A.W. Ashton, R. Yokota, G. John, S. Zhao, S.O. Suadicani, D.C. Spray, J.A. Ware, Inhibition of endothelial cell migration, intercellular communication, and vascular tube formation by thromboxane A(2), J Biol Chem 274 (50) (1999) 35562–35570.
[12] E.M. Battinelli, B.A. Markens, J.E. Italiano Jr., Release of angiogenesis regulatory proteins from platelet alpha granules: modulation of physiologic and pathologic angiogenesis, Blood 118 (5) (2011) 1359–1369.
[13] R.A. Benndorf, E. Schwedhelm, A. Gnann, R. Taheri, G. Kom, M. Didié, A. Steenpass, S. Ergün, R.H. Böger, Isoprostanes inhibit vascular endothelial growth factor-induced endothelial cell migration, tube formation, and cardiac vessel sprouting in vitro, as well as angiogenesis in vivo via activation of the thromboxane A(2) receptor: a potential link between oxidative stress and impaired angiogenesis, Circ Res 103 (9) (2008) 1037–1046.
[14] M. Félétou, R.A. Cohen, P.M. Vanhoutte, T.J. Verbeuren, TP receptors and oxidative stress hand in hand from endothelial dysfunction to atherosclerosis, Adv Pharmacol 60 (2010) 85–106.
[15] Y. Gao, R. Yokota, S. Tang, A.W. Ashton, J.A. Ware, Reversal of angiogenesis in vitro, induction of apoptosis, and inhibition of AKT phosphorylation in endothelial cells by thromboxane A(2), Circ Res 87 (9) (2000) 739–745.

[16] S. Pal, J. Wu, J.K. Murray, S.H. Gellman, M.A. Wozniak, P.J. Keely, M.E. Boyer, T. M. Gomez, S.M. Hasso, J.F. Fallon, E.H. Bresnick, An antiangiogenic neurokinin-B/thromboxane A2 regulatory axis, J Cell Biol 174 (7) (2006) 1047–1058.
[17] Y. Shen, S. Zuo, Y. Wang, H. Shi, S. Yan, D. Chen, B. Xiao, J. Zhang, Y. Gong, M. Shi, J. Tang, D. Kong, L. Lu, Y. Yu, B. Zhou, S.Z. Duan, C. Schneider, C.D. Funk, Y. Yu, Thromboxane Governs the Differentiation of Adipose-Derived Stromal Cells Toward Endothelial Cells In Vitro and In Vivo, Circ Res 118 (8) (2016) 1194–1207.
[18] P.S. Tsou, M.A. Amin, P.L. Campbell, G. Zakhem, B. Balogh, G. Edhayan, R. A. Ohara, E. Schiopu, D. Khanna, A.E. Koch, D.A. Fox, Activation of the Thromboxane A2 Receptor by 8-Isoprostane Inhibits the Pro-Angiogenic Effect of Vascular Endothelial Growth Factor in Scleroderma, J Invest Dermatol 135 (12) (2015) 3153–3162.
[19] H. Amano, Y. Ito, K. Eshima, S. Kato, F. Ogawa, K. Hosono, K. Oba, H. Tamaki, H. Sakagami, M. Shibuya, S. Narumiya, M. Majima, Thromboxane A2 induces blood flow recovery via platelet adhesion to ischaemic regions, Cardiovasc Res 107 (4) (2015) 509–521.
[20] T.O. Daniel, H. Liu, J.D. Morrow, B.C. Crews, L.J. Marnett, Thromboxane A2 is a mediator of cyclooxygenase-2-dependent endothelial migration and angiogenesis, Cancer Res 59 (18) (1999) 4574–4577.
[21] D. Nie, M. Lamberti, A. Zacharek, L. Li, K. Szekeres, K. Tang, Y. Chen, K.V. Honn, Thromboxane A(2) regulation of endothelial cell migration, angiogenesis, and tumor metastasis, Biochem Biophys Res Commun 267 (1) (2000) 245–251.
[22] R. Eckenstaler, A. Ripperger, M. Hauke, M. Petermann, S.A. Hemkemeyer, E. Schwedhelm, S. Ergün, M. Frye, O. Werz, A. Koeberle, H. Braun, R.A. Benndorf, A Thromboxane A(2) Receptor-Driven COX-2-Dependent Feedback Loop That Affects Endothelial Homeostasis and Angiogenesis, Arterioscler Thromb Vasc Biol (2022) Atvbaha121317380.
[23] C. Grashoff, B.D. Hoffman, M.D. Brenner, R. Zhou, M. Parsons, M.T. Yang, M. A. McLean, S.G. Sligar, C.S. Chen, T. Ha, M.A. Schwartz, Measuring mechanical tension across vinculin reveals regulation of focal adhesion dynamics, Nature 466 (7303) (2010) 263–266.
[24] N.R. Reinhard, S.F. van Helden, E.C. Anthony, T. Yin, Y.I. Wu, J. Goedhart, T. W. Gadella, P.L. Hordijk, Spatiotemporal analysis of RhoA/B/C activation in primary human endothelial cells, Sci Rep 6 (2016) 25502.
[25] R.H. Kutner, X.Y. Zhang, J. Reiser, Production, concentration and titration of pseudotyped HIV-1-based lentiviral vectors, Nat Protoc 4 (4) (2009) 495–505.
[26] U.M. Gehling, M. Willems, K. Schlagner, R.A. Benndorf, M. Dandri, J. Petersen, M. Sterneck, J.M. Pollok, D.K. Hossfeld, X. Rogiers, Mobilization of hematopoietic progenitor cells in patients with liver cirrhosis, World J Gastroenterol 16 (2) (2010) 217–224.
[27] T. Korff, H.G. Augustin, Integration of endothelial cells in multicellular spheroids prevents apoptosis and induces differentiation, J Cell Biol 143 (5) (1998) 1341–1352.
[28] H. Braun, M. Hauke, A. Ripperger, C. Ihling, M. Fuszard, R. Eckenstaler, R. A. Benndorf, Impact of DICER1 and DROSHA on the Angiogenic Capacity of Human Endothelial Cells, Int J Mol Sci 22 (18) (2021) 9855.
[29] R. Eckenstaler, R.A. Benndorf, A Combined Acceptor Photobleaching and Donor Fluorescence Lifetime Imaging Microscopy Approach to Analyze Multi-Protein Interactions in Living Cells, Front Mol Biosci 8 (2021), 635548.
[30] K.J. Livak, T.D. Schmittgen, Analysis of relative gene expression data using real-time quantitative PCR and the 2(-Delta Delta C(T)) Method, Methods 25 (4) (2001) 402–408.
[31] A. Ripperger, R.A. Benndorf, The C421A (Q141K) polymorphism enhances the 3'-untranslated region (3'-UTR)-dependent regulation of ATP-binding cassette transporter ABCG2, Biochem Pharmacol 104 (2016) 139–147.
[32] J. Weiss, A. Sauer, M. Herzog, R.H. Böger, W.E. Haefeli, R.A. Benndorf, Interaction of thiazolidinediones (glitazones) with the ATP-binding cassette transporters P-glycoprotein and breast cancer resistance protein, Pharmacology 84 (5) (2009) 264–270.
[33] J. Weil, R. Benndorf, S. Fredersdorf, D.P. Griese, T. Eschenhagen, Norepinephrine upregulates vascular endothelial growth factor in rat cardiac myocytes by a paracrine mechanism, Angiogenesis 6 (4) (2003) 303–309.
[34] S. Deppe, A. Ripperger, J. Weiss, S. Ergün, R.A. Benndorf, Impact of genetic variability in the ABCG2 gene on ABCG2 expression, function, and interaction with AT1 receptor antagonist telmisartan, Biochem Biophys Res Commun 443 (4) (2014) 1211–1217.
[35] F. Michel, J.S. Silvestre, L. Waeckel, S. Corda, T. Verbeuren, J.P. Vilaine, M. Clergue, M. Duriez, B.I. Levy, Thromboxane A2/prostaglandin H2 receptor activation mediates angiotensin II-induced postischemic neovascularization, Arterioscler Thromb Vasc Biol 26 (3) (2006) 488–493.
[36] C.M. Yoon, B.S. Hong, H.G. Moon, S. Lim, P.G. Suh, Y.K. Kim, C.B. Chae, Y.S. Gho, Sphingosine-1-phosphate promotes lymphangiogenesis by stimulating S1P1/Gi/PLC/Ca2+ signaling pathways, Blood 112 (4) (2008) 1129–1138.
[37] J. Sun, W. Huang, S.F. Yang, X.P. Zhang, Q. Yu, Z.Q. Zhang, J. Yao, K.R. Li, Q. Jiang, C. Cao, Gαi1 and Gαi3mediate VEGF-induced VEGFR2 endocytosis, signaling and angiogenesis, Theranostics 8 (17) (2018) 4695–4709.
[38] K.K. Sivaraj, R. Li, J. Albarran-Juarez, S. Wang, D. Tischner, M. Grimm, J. M. Swiercz, S. Offermanns, N. Wettschureck, Endothelial Gαq/11 is required for VEGF-induced vascular permeability and angiogenesis, Cardiovasc Res 108 (1) (2015) 171–180.
[39] L. Zhang, C. DiLizio, D. Kim, E.M. Smyth, D.R. Manning, The G12 family of G proteins as a reporter of thromboxane A2 receptor activity, Mol Pharmacol 69 (4) (2006) 1433–1440.
[40] E.L. Bodmann, A.L. Krett, M. Bünemann, Potentiation of receptor responses induced by prolonged binding of Gα(13) and leukemia-associated RhoGEF, Faseb j 31 (8) (2017) 3663–3676.
[41] K.K. Sivaraj, M. Takefuji, I. Schmidt, R.H. Adams, S. Offermanns, N. Wettschureck, G13 controls angiogenesis through regulation of VEGFR-2 expression, Dev Cell 25 (4) (2013) 427–434.
[42] S. Del Galdo, C. Vettel, D.M. Heringdorf, T. Wieland, The activation of RhoC in vascular endothelial cells is required for the S1P receptor type 2-induced inhibition of angiogenesis, Cell Signal 25 (12) (2013) 2478–2484.